Generation and Suppression of Non-uniform Flow in Scramjet Engines

Hidenori Ben and Toshinori Watanabe
University of Tokyo
Bunkyo-ku Tokyo 113-8656,Japan
watanabe@aero.t.u-tokyo.ac.jp

Key Words : Scramjet Engine, Internal Flow, Shock-Boundary layer Interaction, Boundary Layer Suction

Abstract

In scramjet engines with sidewall compression inlet, it is well known that a non-uniform flow appears since a separated region is generated near the flow centerline on the body side. The separated region is caused by shock-boundary layer interaction and likely to cause un-start phenomena since the flow in the separated region is subsonic and acts as a communication path between the isolator and the combustor. In the present study, the non-uniform flow characteristics in the scramjet inlet-isolator region are numerically studied in detail. Effect of flow suction from body sidewall surface on the non-uniform flow field numerically examined to clarify the flow mechanism to suppress the un-start transition.

Introduction

For realization of forthcoming space planes and hypersonic transports, scramjet engine is expected as one of the appropriate propulsion systems.

Airframe built-in type scramjet engine designed in NASA Langley Research Center utilizes an oblique shock from airframe front edge, and the body-surface boundary layer starting at the front edge inevitably affects the incoming flow of the scramjet engine module.

Two types of inlet are plausible for the scramjet engines for necessary compression. One is sidewall compression type and the other is lateral wall compression type. For the evaluation and performance analysis of the inlets, the flow characteristics must be thoroughly studied including the influence of incoming boundary layers developed on the airframe surface.

Korkegi et al[1] studied pressure rise due to a single fin which assumed a scramjet inlet and indicated that the sidewall compression inlet was less susceptible to the pressure rise due to flow separation than the lateral wall compression inlet. The sidewall compression type was thereby judged feasible as the scramjet inlet.

In the sidewall compression scramjet engine, however, it is well known that non-uniform flow field would appear due to a shock-boundary layer interaction. A separated flow region was observed in this type also near the flow centerline on the body sidewall through the engine flow channel. The separated region is likely to cause un-start phenomenon because the flow in the separated region is subsonic and acts as a communication path between the isolator and the combustor.

On the non-uniformity of the flow field, some intensive researches have been done so far. T. J. Garrison et al[2] studied shock-boundary layer interaction both numerically and experimentally and depicted flow structures in a scramjet inlet. F.Alvi et al[3] visualized shock boundary layer interaction using a conical shadowgraph and examined a region where the shock boundary layer interaction is observed.

The combustion experiment performed by NAL[4] indicated that control of non-uniformity by flow suction could suppress the un-start transition. However, the mechanisms of generation and suppression of non-uniformity in the scramjet engine inlet and isolator are not clarified still now.

In the present study, the non-uniform flow characteristics in the scramjet inlet region are numerically studied. Effect of flow suction from body sidewall surface on the non-uniform flow is numerically examined in detail to clarify the flow mechanism to suppress the un-start transition.

Numerical Method

Numerical Scheme

Navier-Stokes equations were formulated in a cell-vertex finite volume manner. The inviscid terms were discretized with LDFSS (Low Dimension Flux Splitting Scheme). Viscous and diffusion terms were discretized by central difference. Baldwin-Lomax model was used as the turbulence model. Inviscid and source terms of the governing equations were implicitly solved with LU-SGS scheme.

Computational domain

Figure 1 shows schematic view of the computational domain of the inlet isolator in a scramjet engine. The configuration is based on the E2 model used in the subscale wind tunnel for the aerodynamic experiments at NAL Kakuda Research center.

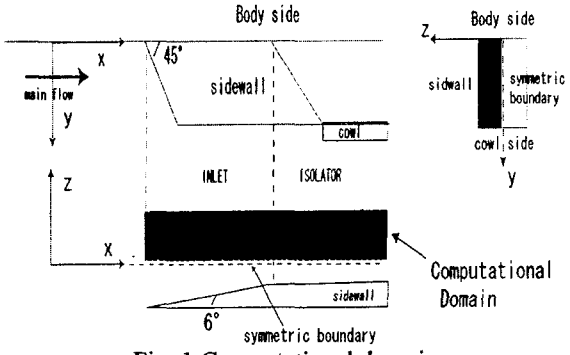

Fig. 1 Computational domain

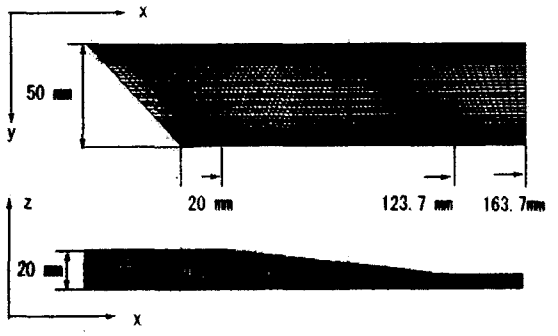

Fig. 2 Computational grid

The E2 model has a sidewall compression inlet whose compression angle is 6 degrees. It has a backward sweep with the angle of 45 degrees at the inlet for the purpose of modifying engine start conditions. A cowl is placed from the inlet of the isolator, so that a part of main flow can spill to adjust the incoming mass flow in the isolator.

The computational grid is shown in Fig. 2. The inlet boundary is located 20 mm upstream position. The height of the flow channel (y-direction) is 50mm and the length of inlet (x-direction) is 123.7 mm. The width of the channel (z-direction) is 40mm, though the computational domain is only the half of it because of the flow symmetry. The length of the isolator is 40 mm at the cowl side and 90mm at the body side, respectively. The difference is due to the backward sweep of the inlet.

Computational conditions

In the present study, M4 flight condition was assumed. Since the main flow was decelerated by oblique shocks on the airframe surface, the inflow Mach number was set to be 2.76 for the computation. Total pressure and total temperature were given to be 612659 (Pa) and 921(K), respectively, as the initial inflow conditions. The velocity distribution in the airframe boundary layer was taken into account in the inlet inflow condition. The boundary layer thickness was assumed to be 0.14 times the inlet height, and the velocity profile was correspondent to a 1/8.5 power law. The profile was identical to the result of the NAL subscale wind-tunnel experiment[5].

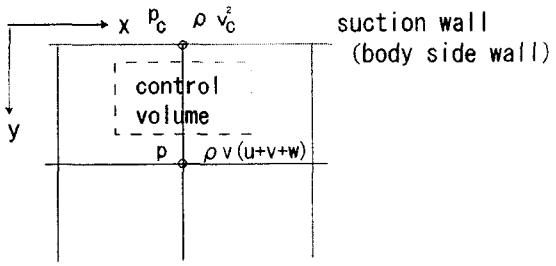

Fig. 3 Schematic view of fluid suction model.

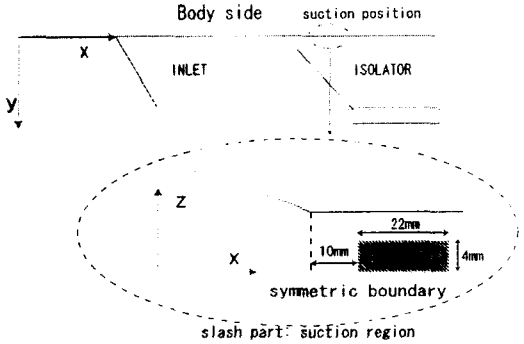

Fig. 4 Location of suction port

Simulation method for flow suction

Figure 3 shows the schematic view of fluid suction model in the present numerical analysis. The air is sucked from the body sidewall. Near the sidewall, the momentum equation in the y-direction is written as

$$P + \rho V(U + V + W) = P_C + \rho V_C^2 . \qquad (1)$$

From Eq. (1), the exhaust velocity Vc is calculated as follows.

$$V_C = \sqrt{\frac{P - P_C}{\rho} + V(U + V + W)} . \qquad (2)$$

(P : static pressure, ρ : density, Pc : static pressure at suction wall, Vc : exhaust velocity, U : x-directional velocity, V : y-directional velocity, W : z-directional velocity)

The flow condition on the wall is determined by adjusting the value of Vc to that calculated through the above equation.

Computational conditions for the case with Suction

In the flow calculation for the case with suction, initial and boundary conditions are identical with those for the base flow simulation. The following suction condition was additionally imposed.

Figure 4 shows the location of the suction. The suction port is made on the body sidewall at 10mm downstream position from the isolator inlet. The computational grid for the suction port is rectangular mesh with 10×10 nodes. On each node in the suction

region, the velocity Vc was determined for the specified value of Pc through Eqs. (1) and (2). The value of Pc was estimated from the inner nodes to obtain the suction flow rate of 3 % of the mean flow.

Results and Discussions

Flow field in the original model

Mach contours and pressure contours in the inlet region are shown in Fig. 5 and Fig. 6 on some typical planes. The plain (A) is located at x/L=0.0, the plain (B) is at x/L=0.5, and the plain (C) is located at x/L = 1.0, where L denotes the length of the inlet. It is clearly shown in the figures that a flow region with low Mach number and low pressure is generated near the body sidewall. The region is seen to rapidly grow in the downstream direction.

Figures 7 and 8 are the Mach contour diagrams on the x-z planes near the body side surface and near the cowl surface, respectively. The shock structure due to sidewall compression is observed near the cowl side

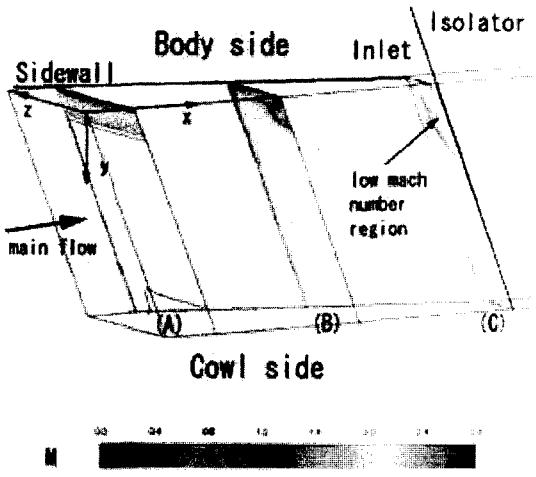

Fig. 5 Mach contour in the inlet

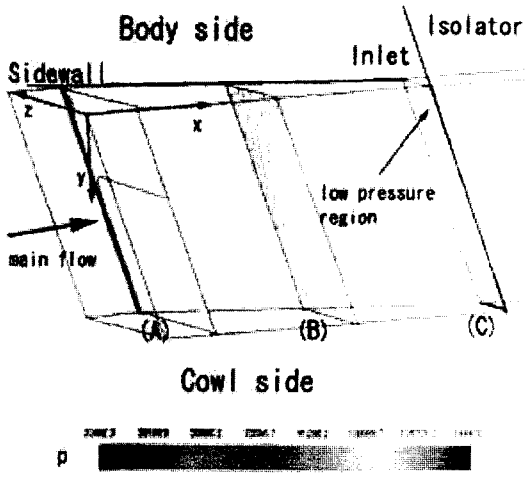

Fig. 6 Pressure contour in the inlet

in Fig. 7. In Fig. 8, however, the structure is not observed near the body side. The difference is attributed to the effect of incoming boundary layer. The flow Mach number is relatively low near the body side due to the boundary layer on the upstream body surface. In Fig. 7, a low Mach number region is observed near the symmetric boundary. The region generates just downstream of the inlet and continues till the end of the isolator.

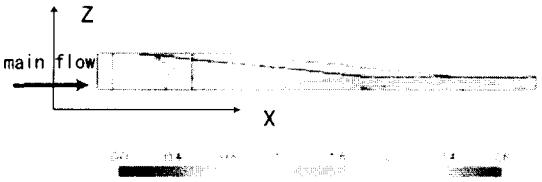

Fig. 7 Mach contour diagram near the body sidewall

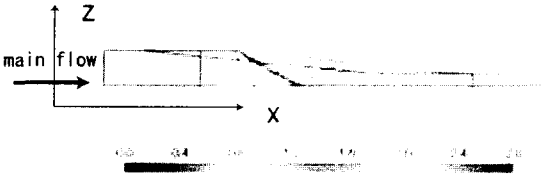

Fig. 8 Mach contour diagram near the cowl surface

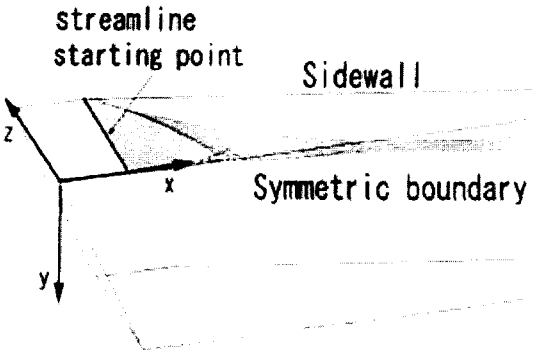

Fig. 9 Streamlines start from a horizontal line near the body sidewall

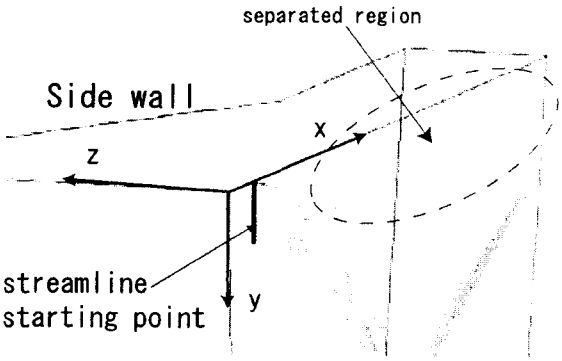

Fig. 10 Streamlines starting from the symmetric plane

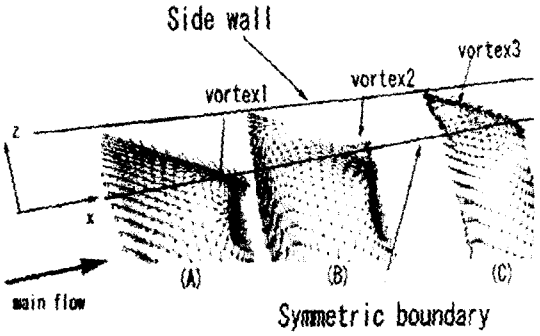

Fig. 11 Velocity vectors near the separated region

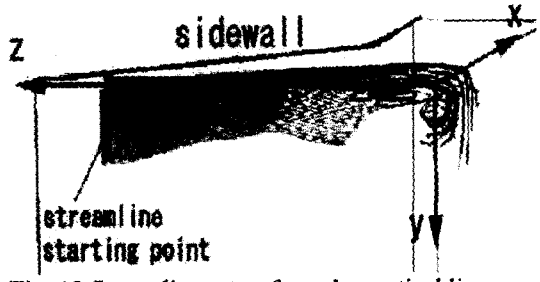

Fig. 12 Streamlines start from the vertical line on the body side surface near the sidewall

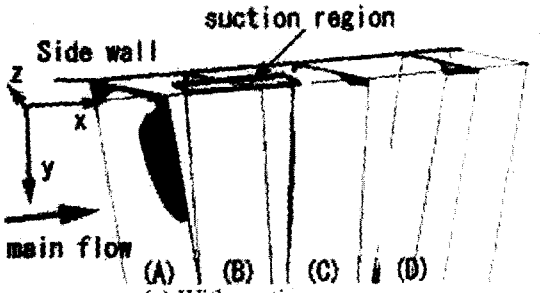

(a) With suction

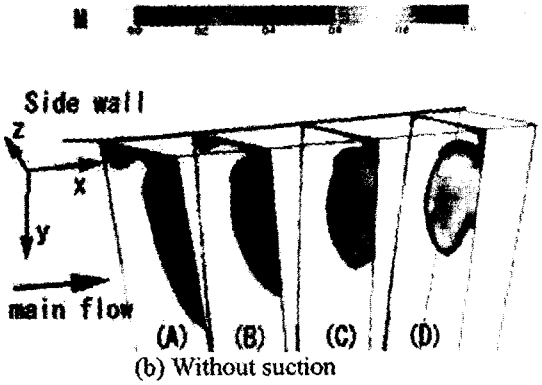

(b) Without suction

Fig. 13 Comparison of Mach number contours near the suction region between the cases with suction and without suction.

Figure 9 shows streamlines start from a horizontal line near the body sidewall. The streamlines start at the front edge of the inlet. The flow directed toward the symmetric boundary is notable near the body sidewall.

The streamlines starting from the symmetric plane are shown in Fig. 10. The streamlines start at the front edge of the inlet. A large region of flow separation is observed on the body sidewall. In Fig. 5 and Fig. 6, a flow region with low Mach number and low pressure was generated near the body sidewall of the central area of the flow channel. The region should be correspondent to the separated region illustrated in Fig. 10.

Velocity vectors near the separated region are shown in Fig. 11 on the three typical y-z planes. The plane (A) is located at x/L=0.41, the plane (B) is at x/L=0.63, and the plane (C) is located at x/L = 0.93. Three longitudinal vortices are seen in the region as indicated in Fig. 11.

Figure 12 shows streamlines start from the vertical line on the body side surface near the sidewall. The streamlines are observed to travel from the sidewall to the central plane of the channel. The flow near the body sidewall reaches the central plane and turns inward toward the cowl side direction to generate the vortex 1.

Vortex 2 shown in Fig. 11 has the rotation of opposite direction to the vortex 1 and is observed in the downstream region of the vortex 1. The vortex is, hence, a secondary vortex induced by the vortex 1. Vortex 3, which has the rotation of opposite direction to vortex 2, is observed on the plane (C). This vortex is generated by the flow from the channel center to the sidewall, which must be induced by the vortex 2. Vortex 3 is thus thought to be a secondary vortex caused by the vortex 2.

Generation of vortex 1 is due to the separated flow that occurs near the body sidewall of the central part of flow channel and the flow incoming from the sidewall to the symmetric boundary. It can also be stated that these vortices are observed in the separated region illustrated in Fig. 10.

Analysis of the case with flow suction

Figure 13 shows comparison of Mach number contour near the suction region between the cases with suction and without suction. Subsonic regions are indicated as the colored areas. The plane (A) is located at x/L=1.00, the plane (B) at x/L = 1.18, the plain (C) at x/L =1.38, and the plane (D) is located at x/L =1.74, where x is the distance from the front edge of inlet and L denotes the length of the inlet. The suction is carried out from x/L = 1.08 to x/L = 1.26. The results show that the low Mach number region disappears at the suction port by the effect of flow suction. The subsonic region reappears on the wall surface in the downstream region of the suction port.

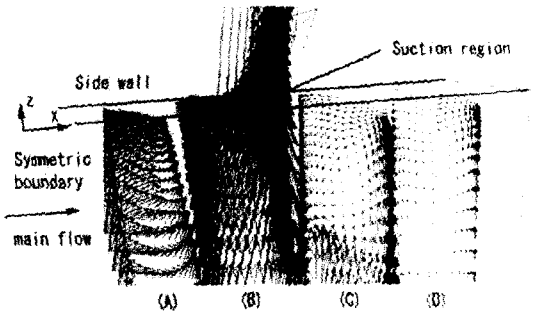

(a) With suction

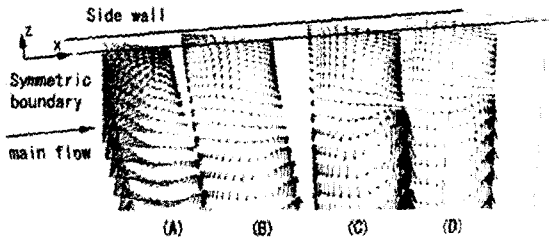

(b) Without suction

Fig. 14 Comparison of velocity vectors near the body side surface in the isolator between the cases with suction and without suction

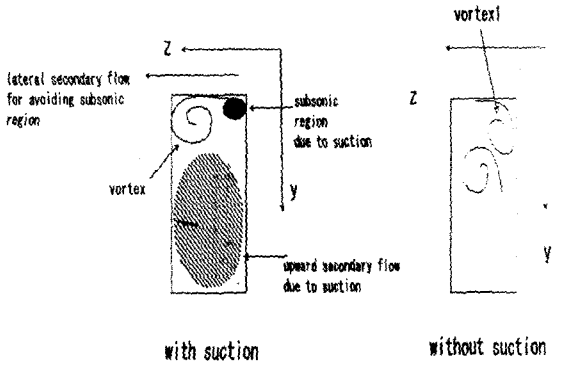

Fig. 15 Sketches of the flow fields at the isolator outlet for both cases with suction and without suction

The favorable effect of the suction on un-start alleviation, found in the experiment of NAL[4], may be attributable to the disappearance of subsonic region, though the detailed mechanism is not yet clear.

In Fig. 14, velocity vectors near the body side surface in the isolator are compared between the cases with suction and without suction The locations of the planes (A) – (D) are identical to those in Fig. 13. In the vector diagrams of Fig. 14 (b), vortex 1 and vortex 3 are still observed in the isolator flow field for the case without suction. Another vortex can be seen below the vortex 1, which should be induced by the vortex 1. In Fig. 14 (a), on the other hand, both the vortex 1 and the vortex 3 disappear from the body

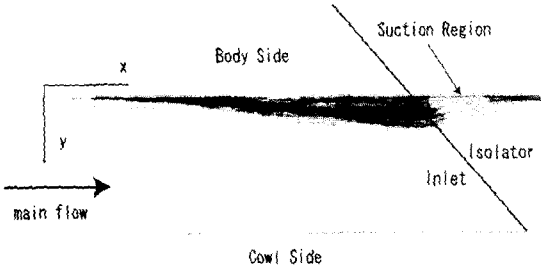

(a) With suction

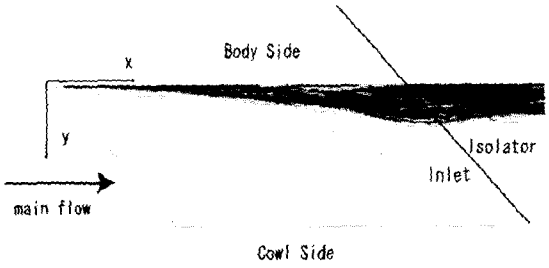

(b) Without suction

Fig. 16 Comparison of streamlines between the cases with suction and without suction.

side flow field. In the downstream region of the suction port, a large vortex appears instead. The vortex has the opposite direction of rotation against that of the vortex 1, and continues to exist at the exit of the isolator. Figure 15 shows sketches of the flow fields at the isolator outlet for both cases with suction and without suction.

Figure 16 shows comparison of streamlines between the cases with suction and without suction. From the comparison between (a) and (b), it is noticed that the separated region generated by the incoming flow near the body side is reduced by the flow suction and the flow exhausted from suction port is accelerated on the suction port. The acceleration might make the subsonic region disappear at the suction port as illustrated in Fig. 13(a).

Total pressure loss characteristics

The total pressure loss was compared between the cases with suction and without suction for considering practical application of the suction technique.

The total pressure loss parameter, π, is defined by

$$\pi = 1 - \frac{\int_A \rho u P dA \Big/ \int_A \rho u dA}{\int_{A_i} \rho u P dA \Big/ \int_{A_i} \rho u dA}, \qquad (3)$$

where P is the total pressure and A denotes the inlet area. The parameter π represents the mass flux weighted total pressure loss coefficient based on the initial condition of the main flow.

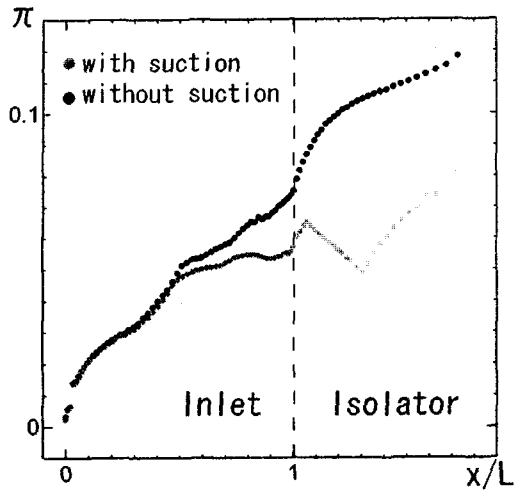

Fig.17 Total pressure loss distribution

Figure 17 shows comparison of the total pressure loss between the cases with suction and without suction. The loss parameter π is plotted against the non-dimensional distance from the front edge of the inlet based on the inlet length, L. From the results, it can be mentioned that the total pressure loss in the case with suction is much lower than that in the case without suction. The reduction of loss is attributed to the suction of the fluids with low pressure in the separated flow region observed above. From the practical point of view, however, the power input for suction must be taken into account, of course.

Conclusions

The internal flow field of scramjet engine inlet and isolator was numerically studied. Effect of flow suction from the body sidewall was investigated with the intention of clarifying the alleviation mechanism of engine un-start phenomenon. The conclusions are summarized as follows.

1. A low Mach number and low pressure flow region appears near the body side surface of engine flow channel. The region rapidly grows in the main flow direction.
2. The low Mach number region is generated by flow separation from the body side surface.
3. In the separated region, three longitudinal vortices are observed. The principal one of them is caused by the flow separation, and it induces the other two secondary vortices.
4. Flow suction from the body side surface in the isolator can suppress the generation and growth of the flow region with low Mach number and low pressure.
5. In the flow field with suction, total pressure loss is reduced.

References

1) Korkegi, R.H et al : Comparison of Shock Induced Two- and Three Dimensional Incipient Turbulent Boundary layer Separation *AIAA Journal Vol13 No4*, 1975, pp.534-535
2) T.J.Garrison et al : Structure of Crossing Shock Wave turbulent Boundary-Layer Interactions, *AIAA Journal Vol31 No12*, 1993, pp.2204-2211
3) F.Alvi : Structure of Swept Shock Wave Boundary Layer Interactions Using Conical Shadowgraphy, *AIAA 90-1644*
4) Kan Kobayashi et al : Suppression of Combustor-Inlet interaction in a scramjet engine under M4 flight condition, *Proceedings of the Annual Meeting and the Forth Symposium on Propulsion System for Reusable Launch Vehicles* ,2003, pp. 179-184 (in Japanese)
5) Tohru Mitani et al : Subscale wind tunnels and supplemental studies of scramjet engine tests *Technical report of national aerospace laboratory TR-1458*, pp. 30-38 (in Japanese)